JACS
JOURNAL OF THE AMERICAN CHEMICAL SOCIETY

Article

pubs.acs.org/JACS

Atomic Structure of Wurtzite CdSe (Core)/CdS (Giant Shell) Nanobullets Related to Epitaxy and Growth

Eva Bladt,[†] Relinde J. A. van Dijk-Moes,[‡] Joep Peters,[‡] Federico Montanarella,[‡] Celso de Mello Donega,[‡] Daniël Vanmaekelbergh,[‡] and Sara Bals*[,†]

[†]Electron Microscopy for Materials Research (EMAT), University of Antwerp, Groenenborgerlaan 171, B-2020 Antwerp, Belgium
[‡]Debye Institute for Nanomaterials Science, University of Utrecht, 3512 JE Utrecht, Netherlands

Supporting Information

ABSTRACT: Heteronanocrystals consisting of a CdSe core and a giant CdS shell have shown remarkable optical properties which are promising for applications in opto-electrical devices. Since these properties sensitively depend on the size and shape, a morphological characterization is of high interest. Here, we present a high angle annular dark field scanning transmission electron microscopy (HAADF-STEM) study of CdSe (core)/CdS (giant shell) heteronanocrystals. Electron tomography reveals that the nanocrystals have a bullet shape, either ending in a tip or a small dip, and that the CdSe core is positioned closer to the tip (or dip) than to the hexagonal base. Based on a high resolution HAADF-STEM study, we were able to determine all the surface facets. We present a heuristic model for the different growth stages of the CdS crystal around the CdSe core.

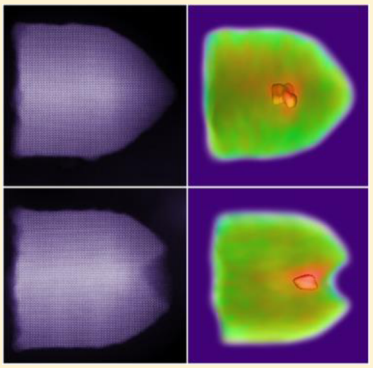

INTRODUCTION

Soon after the first successful synthesis of colloidal CdSe nanocrystals with reasonable photoluminescence quantum yield and size-dispersity,[1] it became clear that the growth of a shell of a higher band gap semiconductor, such as ZnS and CdS, around the core increases the photoluminescence quantum yield and the photochemical stability.[2−6] This has, finally, resulted in synthetic routes for CdSe/X core/shell systems with near-unit photoluminescence quantum yield, applicable as phosphors in LEDS, lasers, and as biological labels.[7−12] As a spin-off of this extensive research, it also became clear that the exciton wave functions and related optical properties could be engineered by the chemical composition and dimensions of the shell. In such a way, CdSe/X heteronanocrystals were reported that (i) displayed a spatial separation of the electron and the hole wave functions,[13,14] (ii) reduced Auger recombination under high excitation densities,[15,16] (iii) reduced blinking when measured on the single quantum dot level.[17,18] This so-called wave function engineering demands a high control of the atomic epitaxy of the shell material on the CdSe core and of the growth of the shell material in case of thicker shells.[19−21] The characterization of CdSe/X shell systems in real space with transmission electron microscopy (TEM) has been very helpful[22] in this, but it should be realized that TEM is a projection method in which valuable information along one dimension is lost (i.e., the direction of the electron beam). For small PbSe (core)/CdSe (shell) heteronanocrystals, it has been shown that a three-dimensional atomic characterization of the heterointerface can be obtained by high angle annular dark-field scanning TEM (HAADF-STEM) tomography.[23] This was enabled by the relative small size of the PbSe/CdSe heteronanocrystals and the large contrast between atomic columns containing Pb or Cd. It is however far from straightforward to determine the three-dimensional atomic structure for much larger heteronanocrystals, e.g., consisting of a core and a giant shell as well as for structures of which the expected contrast between the two materials when imaging in HAADF-STEM mode is not strong.

CdSe (core)/CdS (giant shell) nanocrystals have a remarked scientific and technological importance.[16,21,24] It has been shown that a giant CdS shell results in an enduring photochemical stability and a high photoluminescence quantum yield for excitons and biexcitons, the latter due to strongly reduced Auger recombination.[16,21,25] This makes these systems of interest for high intensity applications in LEDs and lasers. It is clear that the optical properties depend on the shape and dimensions of the CdSe core and the CdS shell, which are on themselves determined by the crystal structure, i.e. zinc blende or wurtzite, and the conditions of the synthesis. The growth of a CdS shell around a zinc blende CdSe core leads to tetrapods, whereas in the case of wurtzite CdSe cores nanowires are formed, due to preferred growth in the [00−1] (*c*-axis) direction.[19] This demonstrates the importance of epitaxy of the CdS crystal on the facets of the CdSe structure.

Here, we present a three-dimensional atomic and chemical characterization of large (30 nm) heteronanocrystals, consisting of a CdSe core embedded in a giant shell of CdS grown by the

Received: June 22, 2016
Published: October 14, 2016

DOI: 10.1021/jacs.6b06443
J. Am. Chem. Soc. 2016, 138, 14288−14293

successive ion layer adhesion and reaction (SILAR) method.[26,27] We made use of a synthesis route to grow multiple CdS layers on wurtzite CdSe cores that leads to large nanocrystals with a bullet shape. The remarkable shape suggests that in this system the atomic epitaxy of CdS on CdSe and the peculiarities of CdS growth are important. In order to understand the initial growth, it is of crucial importance to locate the CdSe core in the bullet-shaped heteronanocrystal. In previous studies of CdSe/CdS core/shell nanorods, the location of CdSe core could be retrieved from 2D TEM techniques such as strain analysis applied to high resolution transmission electron microscopy images[28] and high resolution phase imaging.[29] Due to the large size and anisotropic shape of the bullets, 2D techniques can no longer be used and advanced electron tomography will be applied. Furthermore, the crystallography of the CdS growth is investigated by detailed imaging of the facets present at the surface of the bullet-shaped crystals. This characterization leads to a basic model for the formation of CdSe (core)/CdS (shell) nanobullets.

EXPERIMENTAL SECTION

Synthesis of CdSe Dot in CdS Bulk Nanostructures. The synthesis of the CdSe (core)/CdS (giant shell) heteronanocrystals (HNCs) was performed as follows: CdSe QD seeds were synthesized first,[20] and then a CdS multishell was grown onto CdSe QD seeds via the SILAR method.[10,20] In some cases, a final monolayer of ZnS was grown on top of the CdS; this last step had no effect on the shape of the HNCs. A more detailed description of the synthesis can be found in the Supporting Information.

Optical Measurements. Optical measurements were performed on diluted solutions of washed NCs in anhydrous toluene in quartz cuvettes. Absorption spectra were measured on a double-beam PerkinElmer Lambda 950 UV/vis/NIR spectrophotometer. The photoluminescence spectra were recorded on an Edinburgh Instruments FLS920 spectrofluorometer equipped with a 450 W xenon lamp as excitation source and double grating monochromators. PL decay curves were acquired using an Edinburgh Instruments FLS920 spectrofluorometer and a pulsed diode laser (EPL-375 Edinburgh Instruments, 375 nm, 65 ps pulse width, 1 MHz repetition rate) was used as excitation source. Quantum Yield measurements were performed by reference to a dye, Lumogen red 305 (QY 95%).

X-ray and Electron Diffraction. The low resolution TEM images (SI) and small area electron diffraction (SAED) images were performed on a FEI Tecnai-12 microscope operating at 120 kV. The SAED image is converted to graph which is typical for X-ray diffraction patterns. The angles used in this representation are calibrated with a TlCl reference sample. Samples were prepared by drop-casting a toluene solution of bullet particles onto a carbon-coated copper (400 mesh) TEM grid.

Transmission Electron Microscopy (TEM). Electron tomography experiments were performed using a FEI Tecnai G2 microscope operated at 200 kV. A Fischione tomography holder (model 2020) was used and tilt series were acquired in HAADF-STEM mode over an angular range of ±70° with a tilt increment of 5°. The alignment of the series was performed using the Inspect 3D software.

High resolution HAADF-STEM images were acquired using a cubed FEI Titan microscope operating at 300 kV. A probe semiconvergence angle of ∼21 mrad was used.

RESULTS AND DISCUSSION

Optical Characterization of CdSe/CdS Core/Shell HNCs. Figure S1 (Supporting Information) shows the absorption and emission spectra of the CdSe/CdS core/shell heteronanocrystals in suspension. The extinction sets in at 800 nm and increases considerably with decreasing wavelength, to end with a clear feature at around 500 nm. This feature is due to band edge absorption of the voluminous CdS shell. In most CdSe (core)/CdS (giant shell) systems, the CdS band edge absorption is so dominant that the optical transitions of the CdSe core are hardly visible in a linear plot of the absorptivity vs wavelength. Here, a clear but featureless onset is observed at energies below the band gap of CdS, which can be assigned to light scattering. We remark that the CdSe/CdS core/shell nanocrystals are relatively large colloidal particles, only stabilized by organic capping. As a consequence, small clusters of these bullets might be present in solution acting as light scattering centers. Nasilowski and co-workers attributed the increased absorption at energies below the bandgap of CdS and CdSe to partial alloying of Se and S in the CdSe core.[30] Our results, however, do not provide evidence for this. The luminescence spectrum is centered at around 663 nm with a fwhm of about 55 nm, very much in agreement with the findings of Nasilowski et al. for the so-called graded CdSe (core)/CdS (giant shell) heteronanocrystals.[30]

The PL decay curve (Supporting Information, Figure S2) is far from single exponential. The average lifetime, defined as $\langle\tau\rangle = \Sigma I_i t_i / \Sigma I_i$ with I_i the intensity at delay time t_i after the excitation pulse, decreases from 78.4 ns at 684 nm (the red side of the luminescence spectrum) to 71 ns at 640 nm (the blue side of the spectrum). These long life times suggest that they are dominated by radiative recombination of the exciton. We note that the decay rates are considerably slower than reported for type I CdSe NCs.[31,32]

These findings suggest a considerable delocalization of the electron part of the exciton wave function. Nasilowski et al. report that this leads to such a strong reduction of the Auger recombination that the biexciton PLQY can be as high as the exciton PLQY.[30] We remark that Vanmaekelbergh et al. has reported similar findings for CdSe core/CdS shells systems with thinner shells.[33] In line with the strong biexciton emission, Nasilowski et al. presents single dot emission traces with moderate jittering around a main emission intensity, without the presence of dark periods;[30] such emission traces have been coined "non-blinking" in the literature. We should remark here that the optical properties of CdSe (core)/CdS (giant shell) heteronanocrystals depend in a sensitive way on the epitaxy and atomic details.[30,34,35]

Morphology. Figure 1a shows a HAADF-STEM overview image of the as synthesized CdSe (core)/CdS (giant shell) HNCs. It is clear that the CdSe/CdS core/shell HNCs have an anisotropic shape, with hexagonal and bullet-like projections. In Figure 1b, two hexagonal projections of the HNCs are presented in more detail and an intensity difference in the center can be observed. This is further illustrated by the line profiles in Figure 1c, d acquired along the white rectangles indicated in Figure 1b. Two different types of profiles were observed: Type 1 shows a decrease of the intensity in the center, whereas a higher intensity is observed for type 2. Since the intensity in HAADF-STEM images scales with sample thickness, the presence of a brighter region could be related to an increment in the projected thickness of the HNC. However, the intensity in HAADF-STEM also scales with the atomic number Z. Intensity changes may therefore also be related to the presence of the CdSe core. In order to elucidate the origin of the intensity changes, we applied electron tomography. Tilt series of HAADF-STEM images were acquired for each type of nanoparticle over a range of ±70°.

In Figure 1e–h, the 3D reconstructions are presented, showing two different bullet-type crystal shapes: both have a

DOI: 10.1021/jacs.6b06443
J. Am. Chem. Soc. 2016, 138, 14288–14293

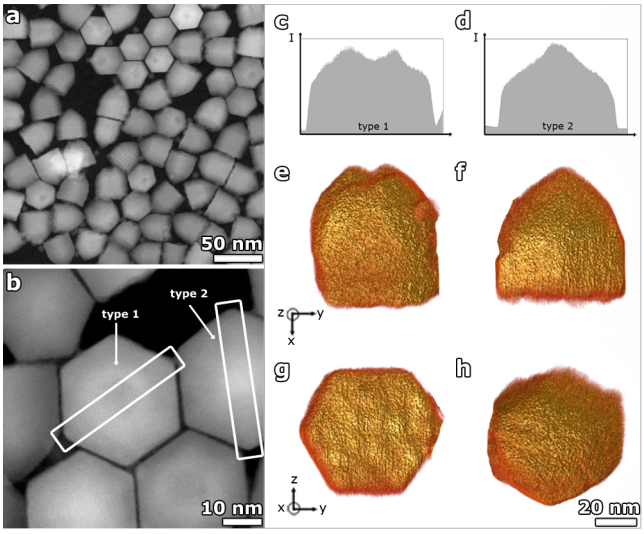

Figure 1. General shape of the CdSe (core)/CdS (giant shell) HNCs. (a) Overview HAADF-STEM image of the CdSe (core)/CdS (giant shell) HNCs demonstrating the bullet shape with a hexagonal basis. (b) HAADF-STEM image of several CdSe/CdS HNCs showing two types of intensity profiles: type 1 shows a lower intensity in the center of the structure, and type 2 a higher intensity. (c,d) Intensity profiles acquired along the white rectangles in (b) are presented, suggesting bullets with a dip or a tip on one end. (e–h) 3D reconstructions unambiguously demonstrate the two different bullet-type crystal shapes: both have a hexagonal base (g, h); however, type 1 ends in a dip (e) and type 2 in a tip (f).

hexagonal base (Figure 1.g and 1.h), but at the other end either a dip (Figure 1.e) or a tip (Figure 1.f) is observed. This explains the intensity differences in the center of the HNCs observed in the 2D HAADF-STEM images. It must be noted that 2D overview images enabled us to estimate that both types of crystal shape are roughly equally present in the samples that we investigated.

Core Location. Previous work on CdSe/CdS core/shell nanorods showed that the CdSe core can be located from 2D high resolution real-space or phase images.[29,36] Recently, X-ray energy dispersive spectroscopy (XEDS) has been applied to visualize the CdSe core in a CdSe/CdS quantum dot in a 2D projection.[35] Because of the larger size of the crystals and the bullet shape, a 3D characterization is indispensable in the present case. Despite of the small difference in atomic number Z between the core and the shell, HAADF-STEM tomography is the preferred technique to investigate the location of the core. Although the use of chemical mapping such as electron energy loss spectroscopy (EELS) or XEDS might be better suited to identify the CdSe core in the HNCs, applying these techniques in 3D was not feasible since the required electron dose induced severe beam damage.

A HAADF-STEM series was acquired over a tilt range of ±70° with a tilt increment of 5°. When inspecting orthoslices through the 3D reconstruction, computed using a conventional algorithm (SIRT), the CdSe core is faintly visible, therefore a correct detection of the position is difficult (Supporting Information, Figure S4). In order to better visualize the CdSe core (Z_{Se} = 34) in the CdS shell (Z_S = 16), we applied a more advanced reconstruction algorithm. The so-called total variation minimization reconstruction algorithm[37] (TVM) is based on the assumption that the gradient of the object under investigation is sparse. As a consequence, edges in the 3D reconstruction will be enhanced. Orthoslices, acquired at the same position as Figure S4 (Supporting Information) are presented in Figure 2c,f. The results show that the core is not

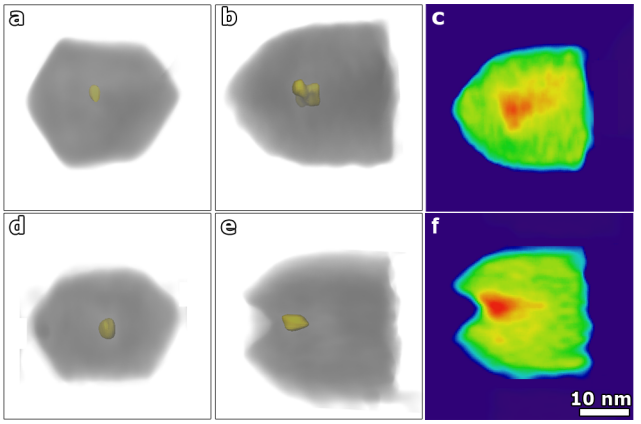

Figure 2. HAADF-STEM tomography on bullet-shaped CdSe/CdS heteronanocrystals to detect the position of the CdSe core. The location of the CdSe core is shown in yellow in the 3D reconstructions of the two types of bullet-shaped HNCs, type 2 with a tip (a,b) and type 1 with a dip (d,e). When applying the total variation minimization reconstruction algorithm, the heavier CdSe core is clearly visible in the orthoslices (c,f).

located in the center of the CdS crystal (Figure 2a,b and d,e), but closer to the tip or dip of the bullets. Previous studies on CdSe/CdS core/shell nanorods also showed an asymmetric position of the CdSe core along the nanorod axis.[19,28,29,38] Overall, the distance between the CdSe core position and the hexagonal base is comparable for both bullet shapes, suggesting a very similar growth process for both morphologies.

Facet Determination. As the two types of bullet-shaped nanocrystals yield a similar position for the CdSe core, the epitaxy and growth of the CdS crystalline shell is expected to be very similar for both types. In order to evaluate the surface energy of both types, the facets of the HNCs need to be identified. Previous studies have shown that the facets of nanocrystals can be investigated by electron tomography.[39−41] Here, this is not straightforward because of the relatively small number of projection images in the tilt series. The lack of information will induce a more rounded shape, which hampers an unambiguous characterization of the facets from a 3D experiment. Therefore, we additionally used direct high resolution HAADF-STEM imaging to determine the facets of the CdSe/CdS bullets. Figure 3 shows a high resolution HAADF-STEM image acquired along the (long) [001] direction. The hexagonal arrangement of the atomic columns (Figure 3c) at the base of the HNC demonstrates that the CdSe/CdS core/shell HNCs have a wurzite crystal structure. Since the wurzite structure is noncentrosymmetric, anisotropic growth is expected, which is confirmed by the position of the CdSe core (see above). However, this is in disagreement with the principles of the SILAR method designed for layer-by-layer growth. It is well possible that, even in the SILAR method, the growth occurs by molecular attachment of CdS units instead of Cd and S in subsequent steps.[42−44] This would preserve the facet polarity and anisotropy. Moreover, a slight excess of the added precursors would enable preferential growth in the polar [00−1], S-terminated direction. Next to the identification of the crystal system, the lateral facets can be examined from the

DOI: 10.1021/jacs.6b06443
J. Am. Chem. Soc. 2016, 138, 14288−14293

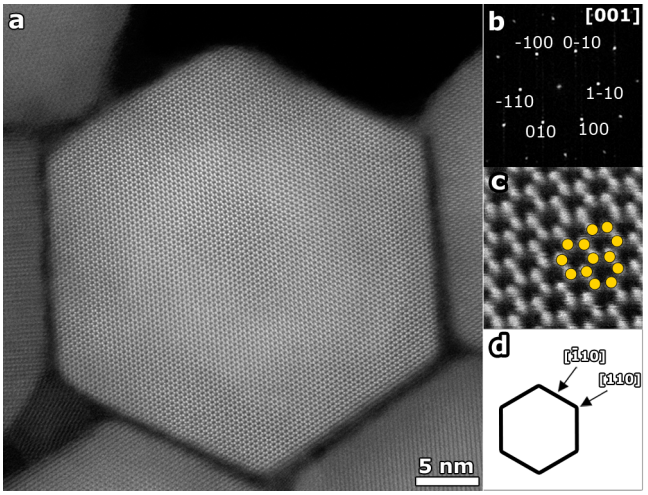

Figure 3. Atomically resolved HAADF-STEM image acquired along the long axis of the bullets. (a) High resolution HAADF-STEM image of a CdSe/CdS bullet-shaped nanocrystal with its corresponding diffractogram (b). The image acquired along the [001] direction shows the hexagonal pattern characteristic for wurtzite. (c) A more detailed view of the atomic arrangement is shown. (d) Schematic of the base of a CdSe/CdS HNC with indication of the [110] and [−110] viewing directions.

high resolution STEM image (Figure 3a) and its corresponding diffractogram (Figure 3b). From these images, the lateral facets are identified as {−110} planes. In Figure 3d, a schematic overview is shown to support the viewing directions with respect to the hexagonal base of a HNC.

In order to investigate the facets that form the tip or the dip, high resolution images acquired along an edge between two lateral facets, corresponding to the [110] direction, are evaluated. In this direction, the angle between a lateral facet and a facet forming the tip can be measured. In this manner, we conclude that the facets at the tip correspond to {1−11} planes. For the type 1 CdSe/CdS bullets with a dip, the d1 and d4 facets (Figure 4c) are identical to the facets forming the tip of the type 2 bullets. The dip forming facets were identified by studying the decrease in intensity in the high resolution HAADF-STEM images due to the presence of the dip. A more detailed comparison is shown in Figure 4b and d. Analyzing the d2 and d3 facets in Figure 4c shows that the d2 facet is parallel to the d4 facet and d3 is parallel to d1. This shows that both types of bullet shapes have identical facets, and a comparable total surface energy.

The complete characterization of the atomic structure and facets of the bullet-shaped CdSe (core)/CdS (giant shell) HNCs suggest a mechanism of CdS epitaxy and growth. It was mentioned above that the growth most probably occurs by attachment of CdS units, rather than separate Cd and S layers. The presence of excess CdS molecular units allows a distinct faster growth of the S-terminated [00−1] facets in the direction of the polar *c*-axis.[43] An atomic simulation of the growth of the giant CdS crystal around the CdSe core is beyond the scope of the present work. Here, we present an intuitive picture, based on the atomic characterization of the bullet-shaped hetero-nanocrystals present above, schematized in Figure 5.

The CdSe core has a wurtzite crystal structure, and induces wurtzite growth of the CdS shell (Supporting Information, Figure S5). In the early stage of the process, epitaxial formation of CdS occurs on all facets, but the growth of wurtzite CdS in

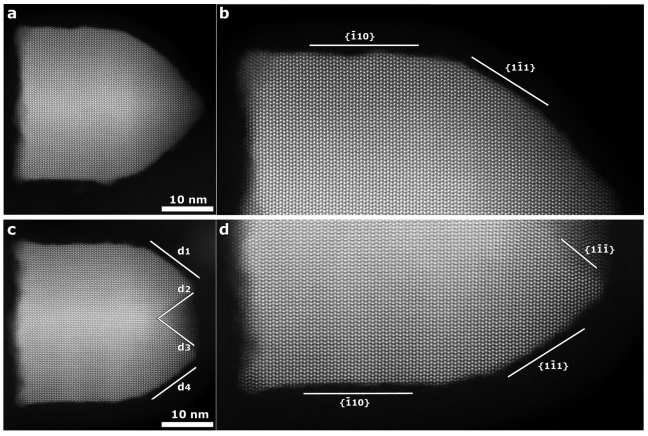

Figure 4. Identification of the facets at the tip or dip of the CdSe/CdS bullet-shaped HNCs. (a,c) High resolution HAADF-STEM images of both types of bullet-shaped nanocrystals, with a more detailed view in (b,d). The lateral facets correspond to [−110] planes. For both types of bullet shapes, the facets originating from the lateral facets toward the dip or tip correspond to [1−11] facets. The type 1 HNCs ending in a dip have additional facets ending in the dip, indicated as (d2 and d3). In (c), it is shown that these facets (d2, d3) are parallel to facet d4 and d1, respectively.

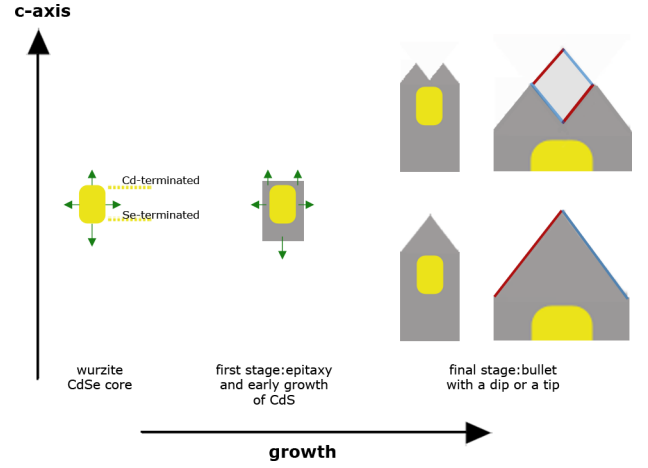

Figure 5. Scheme of the anisotropic growth of the giant CdS shell on the CdSe core. From left to right: slightly elongated wurtzite CdSe crystal core; the green arrows indicate the relative growth rates of the CdS in the [001], [00−1], and [110] directions. In the first stage (Figure S5), there is epitaxy and starting growth of a hexagon-based CdS crystal. Later stages show either a growth in the [001] on top of the crystal accompanied by horizontal ingrowth, resulting in a bullet with a dip; or a growth of the inward facets which result in bullets with a tip. The facets forming the dip are indicated in red and blue to show that a bullet with a tip is build up by exactly the same facets.

the [00−1] direction with a S-terminated facet is faster than in the opposite [001] direction terminated by Cd. This is similar to the growth of CdSe/CdS rods. Such strongly anisotropic growth rates are well documented for wurtzite type crystals.[45−47] In a later stage, the cylindrical crystal shape with hexagonal base typical for wurtzite crystals becomes increasingly pronounced. The growth along the [00−1] is fast with respect to the opposite direction and the 6 lateral directions of the CdS crystal, which grow more slowly. Growth in the direction perpendicular to the *c*-axis can also occur inward (arrows not shown) resulting in a bullet shape with a dip. Possibly, the dip width and depth is gradually reduced by

DOI: 10.1021/jacs.6b06443
J. Am. Chem. Soc. 2016, 138, 14288−14293

inward CdS growth. In any case, stable [1−11] facets present in the dip lead to a low surface energy, and slow growth. It remains ambiguous whether the type 1 and type 2 bullet-shaped heteronanocrystals are equally stable polymorphs, or alternatively, that the type 1 bullets are an unfinished stage, finally resulting into the final bullet-shaped HNCs with a tip. However, based on the facet characterization and equal presence of both types of morphologies, it is suggested that both types are equally stable. The end-facets at the tip indicate that the {1−11} facets are more stable than the Cd-terminated {001} facets.

CONCLUSIONS

CdSe/CdS HNCs with a bullet shape were found to end either with a tip or dip. Using electron tomography the 3D location of the CdSe core in CdSe/CdS HNCs was found to be located at a position closer to the tip or dip. By HAADF-STEM imaging, it was found that the two morphologies are built up by the same facets. Since the facets forming the tip or dip always correspond to {1−11} facets, the surface energies for both morphologies are equal.

ASSOCIATED CONTENT

Supporting Information

The Supporting Information is available free of charge on the ACS Publications website at DOI: 10.1021/jacs.6b06443.

Detailed description of the synthesis, quantum yield, absorption and photoluminescence spectra, decay curves, X-ray and electron diffraction results, orthoslices through the SIRT reconstruction and a 3D visualization of the first stage of the CdSe/CdS nanobullets (PDF)

AUTHOR INFORMATION

Corresponding Author

*sara.bals@uantwerpen.be

Notes

The authors declare no competing financial interest.

ACKNOWLEDGMENTS

S.B. acknowledges financial support from European Research Council (ERC Starting Grant #335078-COLOURATOMS). D.V. wishes to acknowledge the Dutch Foundation for Fundamental Research on Matter (FOM) in the programme "Designing Dirac Carriers in Semiconductor Superstructures". E.B. gratefully acknowledges financial support by the Flemish Fund for Scientific Research (FWO Vlaanderen).

REFERENCES

(1) Murray, C. B.; Norris, D. J.; Bawendi, M. G. *J. Am. Chem. Soc.* **1993**, *115*, 8706.
(2) Hines, M. a.; Guyot-Sionnest, P. *J. Phys. Chem.* **1996**, *100*, 468.
(3) Dabbousi, B. O.; Rodriguez-Viejo, J.; Mikulec, F. V.; Heine, J. R.; Mattoussi, H.; Ober, R.; Jensen, K. F.; Bawendi, M. G. *J. Phys. Chem. B* **1997**, *101*, 9463.
(4) Peng, X.; Schlamp, M. C.; Kadavanich, A. V.; Alivisatos, A. P. *J. Am. Chem. Soc.* **1997**, *119*, 7019.
(5) Banin, U.; Bruchez, M.; Alivisatos, A. P.; Ha, T.; Weiss, S.; Chemla, D. S. *J. Chem. Phys.* **1999**, *110*, 1195.
(6) Revaprasadu, N.; Azad Malik, M.; O'Brien, P.; Wakefield, G. *Chem. Commun.* **1999**, No. c, 1573.
(7) Reiss, P.; Bleuse, J.; Pron, A. *Nano Lett.* **2002**, *2*, 781.
(8) Mekis, I.; Talapin, D. V.; Kornowski, A.; Haase, M.; Weller, H. *J. Phys. Chem. B* **2003**, *107*, 7454.
(9) Talapin, D. V.; Mekis, I.; Götzinger, S.; Kornowski, A.; Benson, O.; Weller, H. *J. Phys. Chem. B* **2004**, *108*, 18826.
(10) Xie, R.; Kolb, U.; Li, J.; Basché, T.; Mews, A. *J. Am. Chem. Soc.* **2005**, *127*, 7480.
(11) Zavelani-Rossi, M.; Lupo, M. G.; Krahne, R.; Manna, L.; Lanzani, G. *Nanoscale* **2010**, *2*, 931.
(12) Chen, O.; Zhao, J.; Chauhan, V. P.; Cui, J.; Wong, C.; Harris, D. K.; Wei, H.; Han, H.-S.; Fukumura, D.; Jain, R. K.; Bawendi, M. G. *Nat. Mater.* **2013**, *12*, 445.
(13) Piryatinski, A.; Ivanov, S. A.; Tretiak, S.; Klimov, V. I. *Nano Lett.* **2007**, *7*, 108.
(14) Allione, M.; Ballester, A.; Li, H.; Comin, A.; Movilla, J. L.; Climente, J. I.; Manna, L.; Moreels, I. *ACS Nano* **2013**, *7*, 2443.
(15) Mangum, B. D.; Wang, F.; Dennis, A. M.; Gao, Y.; Ma, X.; Hollingsworth, J. A.; Htoon, H. *Small* **2014**, *10*, 2892.
(16) Htoon, H.; Malko, A. V.; Bussian, D.; Vela, J.; Chen, Y.; Hollingsworth, J. A.; Klimov, V. I. *Nano Lett.* **2010**, *10*, 2401.
(17) Malko, A. V.; Park, Y.-S.; Sampat, S.; Galland, C.; Vela, J.; Chen, Y.; Hollingsworth, J. A.; Klimov, V. I.; Htoon, H. *Nano Lett.* **2011**, *11*, 5213.
(18) Zhao, J.; Chen, O.; Strasfeld, D. B.; Bawendi, M. G. *Nano Lett.* **2012**, *12*, 4477.
(19) Talapin, D. V.; Nelson, J. H.; Shevchenko, E. V.; Aloni, S.; Sadtler, B.; Alivisatos, A. P. *Nano Lett.* **2007**, *7*, 2951.
(20) Greytak, A. B.; Allen, P. M.; Liu, W.; Zhao, J.; Young, E. R.; Popović, Z.; Walker, B.; Nocera, D. G.; Bawendi, M. G. *Chem. Sci.* **2012**, *3*, 2028.
(21) Christodoulou, S.; Vaccaro, G.; Pinchetti, V.; De Donato, F.; Grim, J. Q.; Casu, A.; Genovese, A.; Vicidomini, G.; Diaspro, A.; Brovelli, S.; Manna, L.; Moreels, I. *J. Mater. Chem. C* **2014**, *2*, 3439.
(22) van Embden, J.; Jasieniak, J.; Mulvaney, P. *J. Am. Chem. Soc.* **2009**, *131*, 14299.
(23) Bals, S.; Casavola, M.; van Huis, M. A.; Van Aert, S.; Batenburg, K. J.; Van Tendeloo, G.; Vanmaekelbergh, D. *Nano Lett.* **2011**, *11*, 3420.
(24) Mangum, B. D.; Sampat, S.; Ghosh, Y.; Hollingsworth, J. a; Htoon, H.; Malko, A. V. *Nanoscale* **2014**, *6*, 3712.
(25) Pal, B. N.; Ghosh, Y.; Brovelli, S.; Laocharoensuk, R.; Klimov, V. I.; Hollingsworth, J. A.; Htoon, H. *Nano Lett.* **2012**, *12*, 331.
(26) Qu, L.; Peng, Z. A.; Peng, X. *Nano Lett.* **2001**, *1*, 333.
(27) Li, J. J.; Wang, Y. A.; Guo, W.; Keay, J. C.; Mishima, T. D.; Johnson, M. B.; Peng, X. *J. Am. Chem. Soc.* **2003**, *125*, 12567.
(28) Carbone, L.; Nobile, C.; De Giorgi, M.; Della Sala, F.; Morello, G.; Pompa, P.; Hytch, M.; Snoeck, E.; Fiore, A.; Franchini, I. R.; Nadasan, M.; Silvestre, A. F.; Chiodo, L.; Kudera, S.; Cingolani, R.; Krahne, R.; Manna, L. *Nano Lett.* **2007**, *7*, 2942.
(29) McBride, J.; Treadway, J.; Feldman, L. C.; Pennycook, S. J.; Rosenthal, S. J. *Nano Lett.* **2006**, *6*, 1496.
(30) Nasilowski, M.; Spinicelli, P.; Patriarche, G.; Dubertret, B. *Nano Lett.* **2015**, *15*, 3953.
(31) van Driel, A. F.; Allan, G.; Delerue, C.; Lodahl, P.; Vos, W. L.; Vanmaekelbergh, D. *Phys. Rev. Lett.* **2005**, *95*, 236804.
(32) de Mello Donegá, C.; Koole, R. *J. Phys. Chem. C* **2009**, *113*, 6511.
(33) Vanmaekelbergh, D.; van Vugt, L. K.; Bakker, H. E.; Rabouw, F. T.; Nijs, B.; van Dijk-Moes, R. J. A.; van Huis, M. A.; Baesjou, P. J.; van Blaaderen, A. *ACS Nano* **2015**, *9*, 3942.
(34) Ghosh, Y.; Mangum, B. D.; Casson, J. L.; Williams, D. J.; Htoon, H.; Hollingsworth, J. A. *J. Am. Chem. Soc.* **2012**, *134*, 9634.
(35) Orfield, N. J.; McBride, J. R.; Wang, F.; Buck, M. R.; Keene, J. D.; Reid, K. R.; Htoon, H.; Hollingsworth, J. A.; Rosenthal, S. J. *ACS Nano* **2016**, *10*, 1960.
(36) Bertoni, G.; Grillo, V.; Brescia, R.; Ke, X.; Bals, S.; Catellani, A.; Li, H.; Manna, L. *ACS Nano* **2012**, *6*, 6453.
(37) Goris, B.; Roelandts, T.; Batenburg, K. J.; Heidari Mezerji, H.; Bals, S. *Ultramicroscopy* **2013**, *127*, 40.
(38) van der Stam, W.; Bladt, E.; Rabouw, F. T.; Bals, S.; de Mello Donega, C. *ACS Nano* **2015**, *9*, 11430.

DOI: 10.1021/jacs.6b06443
J. Am. Chem. Soc. 2016, 138, 14288−14293

(39) Weyland, M.; Yates, T. J. V.; Dunin-Borkowski, R. E.; Laffont, L.; Midgley, P. A. *Scr. Mater.* **2006**, *55*, 29.
(40) González, J. C.; Hernández, J. C.; López-Haro, M.; del Río, E.; Delgado, J. J.; Hungría, A. B.; Trasobares, S.; Bernal, S.; Midgley, P. A.; Calvino, J. J. *Angew. Chem.* **2009**, *121*, 5417.
(41) Goris, B.; Bals, S.; Van den Broek, W.; Carbó-Argibay, E.; Gómez-Graña, S.; Liz-Marzán, L. M.; Van Tendeloo, G. *Nat. Mater.* **2012**, *11*, 930.
(42) Liu, H.; Owen, J. S.; Alivisatos, A. P. *J. Am. Chem. Soc.* **2007**, *129*, 305.
(43) de Mello Donegá, C. *Chem. Soc. Rev.* **2011**, *40*, 1512.
(44) Abe, S.; Čapek, R. K.; De Geyter, B.; Hens, Z. *ACS Nano* **2012**, *6*, 42.
(45) Manna, L.; Milliron, D. J.; Meisel, A.; Scher, E. C.; Alivisatos, A. P. *Nat. Mater.* **2003**, *2*, 382.
(46) Manna, L.; Wang; Cingolani, R.; Alivisatos, A. P. *J. Phys. Chem. B* **2005**, *109*, 6183.
(47) Moore, D.; Wang, Z. L. *J. Mater. Chem.* **2006**, *16*, 3898.

DOI: 10.1021/jacs.6b06443
J. Am. Chem. Soc. 2016, 138, 14288−14293